Förster resonance energy transfer between individual semiconductor nanocrystals and an InP film

Chiara Sinito, Xavier Quélin, Nathalie Simon, Pierrick Gautier, Anne-Marie Gonçalves, Stéphanie Buil, Jean-Pierre Hermier, Damien Aureau

Förster resonance energy transfer between individual semiconductor nanocrystals and an InP film

Chiara Sinito
Xavier Quélin
Nathalie Simon
Pierrick Gautier
Anne-Marie Gonçalves
Stéphanie Buil
Jean-Pierre Hermier
Damien Aureau

SPIE.

Förster resonance energy transfer between individual semiconductor nanocrystals and an InP film

Chiara Sinito,[a,b,*] Xavier Quélin,[b] Nathalie Simon,[a] Pierrick Gautier,[a] Anne-Marie Gonçalves,[a] Stéphanie Buil,[b] Jean-Pierre Hermier,[b,c] and Damien Aureau[a]

[a]Université de Versailles Saint-Quentin-en-Yvelines, Institut Lavoisier de Versailles, CNRS, Université Paris Saclay, UMR8180, 45 Avenue des Etats-Unis, 78035 Versailles, France
[b]Université de Versailles Saint-Quentin-en-Yvelines, Groupe d'Etude de la Matière Condensée, CNRS, Université Paris Saclay, UMR8635, 45 Avenue des Etats-Unis, 78035 Versailles, France
[c]Institut Universitaire de France, 103 Boulevard Saint-Michel, 75005 Paris, France

Abstract. The modification of the radiative decay of a single emitter in close vicinity to a dielectric interface is investigated by studying the photoluminescence (PL) decay dynamics of colloidal semiconductor nanocrystals (NCs) deposited on semiconductor surfaces. The PL decay lifetimes of single CdSe/CdS NCs spin-coated on InP surfaces passivated with thin oxide layers are measured. Electrochemical passivation of the InP surfaces with oxide layers of different thicknesses enables to study the influence of the distance between the semiconductor surface and the NC on the lifetime. A shortening of the PL decay lifetimes of the NCs with respect to their lifetimes on glass strongly suggests the opening of recombination channels for the photogenerated exciton, which we attribute to energy transfer between the NC and the semiconductor. We also experimentally show the influence of the orientation of the NC with respect to the semiconductor surface on the coupling. © *2016 Society of Photo-Optical Instrumentation Engineers (SPIE)* [DOI: 10.1117/1.JNP.10.046014]

Keywords: semiconductor nanocrystals; photoluminescence; III-V semiconductors; energy transfer.

1 Introduction

Energy transfer (ET) can strongly modify the spontaneous emission decay rate of an excited fluorophore (donor), resulting in a decrease of its photoluminescence (PL) intensity as the excitation energy is transferred to an acceptor molecule.[1] Resonant ET occurs without the appearance of a photon and can result from different interaction mechanisms, such as intermolecular orbital overlap and/or Coulombic interaction. All these mechanisms require that the emission spectrum of the donor and the absorption spectrum of the acceptor overlap.[2] Resonant ET based on long-range dipole–dipole interactions was first treated by Förster[3] and is referred to as Förster resonant energy transfer (FRET). The rate of FRET is proportional to $1/r^6$, r being the distance between the two fluorophores, and the distance at which FRET is 50% efficient is in the range of 2 to 6 nm.

Radiative energy transfer (RET) occurs through the absorption by an acceptor of the photon emitted by a donor. This transfer does not require any interaction between the two molecules but still depends on the spectral overlap and on the concentration of the molecules.[2]

The production of free electron–hole pairs in a ground-state bulk semiconductor by ET from an excited fluorophore in its close vicinity has been treated by Dexter et al.[4,5] The electric dipole–dipole coupling between the sensitizer and the bulk acceptor has been treated theoretically by

---

*Address all correspondence to: Chiara Sinito, E-mail: sinito@pdi-berlin.de

combining the Förster–Dexter theory with simple band models[5] and the results have been compared to the classical treatment of ET derived by Chance et al.[6]

The transfer of the exciton energy into the electron–hole pair of a bulk semiconductor acceptor can occur through both RET and nonradiative energy transfer (NRET).[5,6] RET occurs via the preferential decay of the exciton into photonic modes, which propagate only within the underlying semiconductor, whereas NRET consists in the direct production of electron–hole pairs in the semiconductor by the oscillating electrostatic-like dipole field of the exciton.

As a consequence of its strong dependence on the distance between the donor and the acceptor, NRET is efficient within a few nanometers, whereas RET can occur within several tens of nanometers.[1,2]

Recently, dye-sensitization of inorganic semiconductors has gained interest, and ET has enabled the design of hybrid nanostructures involving several kinds of organic and inorganic components with the role of energy donor and acceptor for optoelectronic and/or photovoltaic applications.[7–11]

Hybrid nanostructured systems based on ET combine nanostructured materials with a large absorption cross section in the visible part of the solar spectrum with high mobility semiconductor layers. ET, enabled by a near-field electromagnetic interaction, generates an electron–hole pair in the semiconductor layer.[5] The single charge carriers are then separated and collected within the high mobility semiconductor component, avoiding the issues related to transport through the interface, which affect charge-transfer-based organic bulk-heterojunction systems.[12]

Among the absorber materials suitable for light harvesting and energy conversion, colloidal nanocrystals (NCs) are very good candidates due to a large absorption cross section in the visible range,[13] an ease of chemical synthesis and manipulation, high PL quantum yield, and an extraordinary photostability against photobleaching compared to organic molecules.[14] In addition to a large range of applications, such as biological labeling,[15] light-emitting diodes, and laser technologies,[16] ET between CdSe/ZnS NCs and semiconductor materials has been demonstrated for thick silicon substrates[7,9] and for ultrathin silicon nanomembranes.[8]

Binary III-V semiconductors, such as InP and GaAs, present adaptable optical properties, high switching speed, and low supply voltages,[17] which are advantageous for their integration in optoelectronic and photovoltaic devices. In particular, InP is characterized by a high electron saturation velocity, a high thermal conductivity, and also a large mobility for the charge carriers, up to 5400 cm^2 V^{-1} s^{-1} for the electrons and up to 200 cm^2 V^{-1} s^{-1} for the holes.[18]

In this paper, we report on ET between core/shell CdSe/CdS NCs and InP surfaces passivated with thin oxide layers. We study the PL decay dynamics of the NCs at the single emitter level, getting rid of the average effects due to size dispersion. As detailed below, a wide range of couplings between the NCs and the passivated surfaces is explored, providing fruitful insight into the radiative lifetime modifications of an electric dipole in close vicinity of a polarizable environment. The paper is organized as follow. First, the theoretical treatment of the spontaneous emission of an electric dipole close to a dielectric interface is reviewed. Then the passivation of the InP surfaces, performed by electrochemical treatment, is described. The characteristics of the CdSe/CdS NCs and the experimental setup for the PL measurements are briefly described as well. In Sec. 4, the PL decay dynamics of the NCs deposited on the passivated InP surfaces is discussed. A reduction of the PL decay lifetime of the NCs is observed, suggesting the opening of recombination channels for the photogenerated exciton.

2 Spontaneous Emission of an Electric Dipole in Close Vicinity of a Dielectric Interface

It is well known that the optical environment of an emitter determines its emission pattern[19,20] as well as the radiative lifetime of its excited state.[21–23] If the density of states of the electromagnetic modes $\rho(\nu)$ in the vicinity of the emitter varies only slightly around the transition frequency ν, it is possible to calculate exactly, in the frame of the classical theory of the radiation of an oscillating electric dipole, the modification of the spontaneous emission rate when the emitter is close to a dielectric interface.[23] The expression $\frac{L(z)}{L(z \to \infty)}$ of the total power radiated by a classical oscillating dipole of arbitrary orientation embedded in a medium 1 and located at a distance z from a

medium 2 of different dielectric permittivity normalized to the total power radiated when the dipole is located in an unbound homogeneous medium ($z \to \infty$) has been derived by Lukosz and Kunz.[23]

According to the correspondence principle, the quantum theoretical expression of the power radiated by spontaneous emission can be obtained from the classical expression by replacing the dipole moment with the matrix element of the corresponding transition, leading to $\alpha = \frac{k_{rad}(z)}{k_{rad}(z \to \infty)} = \frac{L(z)}{L(z \to \infty)}$, where $k_{rad}(z)$ and $k_{rad}(z \to \infty)$ represent the radiative emission rate of the dipole transition at a distance z from medium 2 and in an unbound homogeneous medium, respectively.

The exact expression of α for an electric dipole parallel ($\alpha_\parallel$) or perpendicular ($\alpha_\perp$) to a dielectric interface has been derived within the same study.[23] The information on the dielectric environment is contained in the reflection coefficients, which appear in the expressions of $\alpha_\parallel$ and $\alpha_\perp$.

The photogenerated exciton in an NC can be treated as a classical point-like dipole located in the center of the NC. In an NC with a wurtzite crystal structure, as the NCs studied in this work, the fundamental transition is degenerate with incoherent σ^+ and σ^- transitions[24] in the plane perpendicular to the crystalline axis of the wurtzite crystal structure (c-axis).[25] Therefore, the classical dipole always lies within this plane, but its direction of rotation is not defined, and so it is referred to as a two-dimensional (2-D) or degenerate dipole. The 2-D dipole can be decomposed on a two-axis orthogonal basis lying in the plane perpendicular to the c-axis, and its orientation with respect to an interface is defined by the angle θ between the normal to the interface and the c-axis (Fig. 1).

Since we are interested in the way the NC is coupled to the InP surface, we consider how a dielectric interface at distance z from a 2-D electric dipole modifies its radiative lifetime compared to the case when the dipole is located in an infinite homogeneous medium ($z \to \infty$), which is described by α.

For a 2-D dipole in close vicinity to a dielectric interface, two configurations can be identified. If both components of the dipole lie in the plane of the interface, $\alpha = \alpha_\parallel$, whereas if one of the two components of the dipole lies in the plane of the interface while the other one lies perpendicular to it, $\alpha = \frac{1}{2}(\alpha_\parallel + \alpha_\perp)$.[23] All the possible orientations of the dipole are comprised between these two extreme cases, which directly translates into different degrees of coupling between the dipole and the interface. The normalized spontaneous emission rate for an ensemble of randomly oriented dipoles in close vicinity to a dielectric interface is $\langle \alpha \rangle = \frac{2}{3}\alpha_\parallel + \frac{1}{3}\alpha_\perp$. The passivated InP surfaces studied here are layered dielectric systems comprising the interfaces air/oxide and oxide/InP and the expressions of the reflection coefficients can be found in Ref. 26. The value of the complex dielectric function of InP at the emission wavelength of the NCs, $\lambda = 620$ nm, is $\varepsilon(\text{InP}) = 12.493 + i2.252$,[27] whereas for the refractive index of the passivating oxide, we have chosen the one of stoichiometric composition $\text{InP}_{0.6}\text{O}_{2.5}$, $n(\text{InP}_{0.6}\text{O}_{2.5}) = 1.616$.[28] We set $z = 12$ nm as the distance between the dipole and the interface, which corresponds to
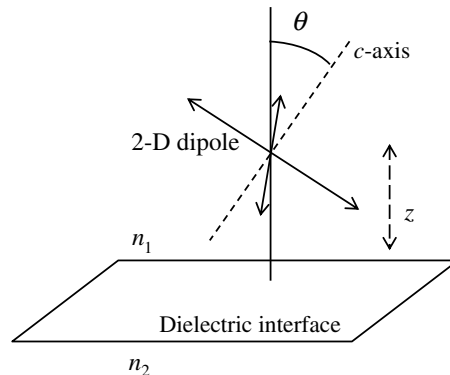

Fig. 1 Scheme of a 2-D electric dipole located in a homogeneous medium of refractive index n_1 at a distance z from a medium of refractive index n_2. The orientation of the dipole with respect to the interface is defined by the angle θ between the crystalline axis and the normal to the planar interface.
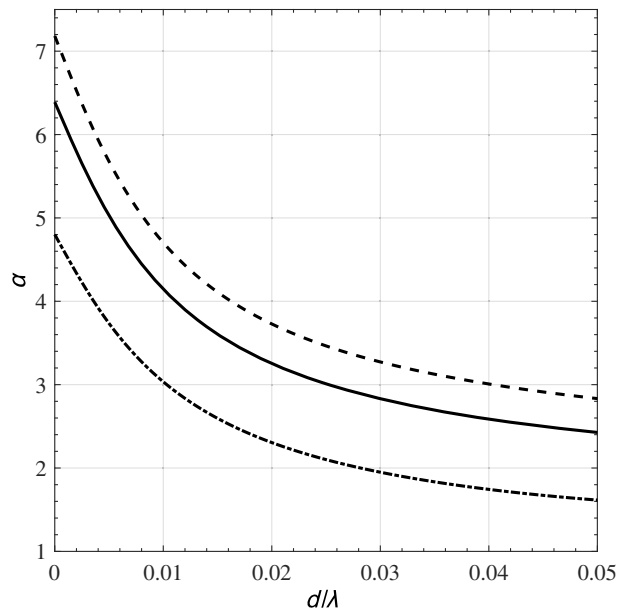
Fig. 2 Simulation of $\alpha = \alpha_\parallel$ (dashed dotted line), $\langle\alpha\rangle = \frac{2}{3}\alpha_\parallel + \frac{1}{3}\alpha_\perp$ (plain line), and $\alpha = \frac{1}{2}(\alpha_\parallel + \alpha_\perp)$ (dashed line) for $z = 12$ nm and $\lambda = 620$ nm as a function of the thickness of the spacer normalized to the emission wavelength of the NCs, d/λ, up to $d = 31$ nm.

an NC of diameter 20 nm surrounded by organic ligands of 2-nm length. The expressions of $\alpha = \alpha_\parallel$ and $\alpha = \frac{1}{2}(\alpha_\parallel + \alpha_\perp)$ as a function of the thickness of the oxide layer normalized to the emission wavelength of the NCs, d/λ, are represented in Fig. 2. The case of an ensemble of randomly oriented dipoles $\langle\alpha\rangle = \frac{2}{3}\alpha_\parallel + \frac{1}{3}\alpha_\perp$ is also shown.

From the curves of Fig. 2, one can see that, for the same value of d/λ, the strongest coupling between the NC and the dielectric surface corresponds to $\alpha = \frac{1}{2}(\alpha_\parallel + \alpha_\perp)$ (dashed line), whereas the weakest coupling occurs for $\alpha = \alpha_\parallel$ (dashed dotted line). The curve corresponding to an ensemble of randomly oriented dipoles (plain line) lies within these two curves.

This theoretical frame is used for the interpretation of the PL decay lifetimes of the NCs on the passivated InP surfaces, discussed below. In Sec. 3, the passivation of the InP surfaces is described.

3 Experimental Results

3.1 *Passivation of the InP Surfaces*

Spontaneous surface oxidation and related high side reactivity result in a high density of traps at the InP surfaces and interfaces, which strongly affects the optical and electrical properties of InP and InP-based devices.[29] Since the stability of the optoelectronic devices based on InP is strongly dependent on the evolution of its electrical and chemical properties, the passivation of InP is a necessary step prior to any integration of InP in optoelectronic devices. There exist several ways of stabilizing the surface chemistry of InP. In the last decades, controlled growths of oxides have been tested, using either dry or wet methods to passivate InP and the electrical properties of the resulting InP/InP$_{oxide}$ interfaces have been largely studied.[30,31] In this work, electrochemical oxidation has been chosen for the passivation of InP for its efficiency in avoiding air aging of the treated surfaces, thanks to the blocking behavior of the resulting thin oxide layers.[29] According to the adopted experimental conditions, such as electrolyte composition, pH, current density, or time, very different oxide layers are grown.[30–33] In the present paper, the anodic treatment of the InP surfaces has been performed in a borate buffered solution at pH 9 leading to the growth of an "InPO$_4$-like" layer with good chemical and electrical properties.[29,34,35] By varying the time and/or the current density, the thickness of the resulting oxide layer can be controlled,[35]

which is of importance in our study since it determines the distance between the absorber material and the semiconductor surface.

The InP bare surfaces are purchased from the company Sumitomo Electric and are n-doped, with a dopant concentration of $10^{18}/cm^3$. On these surfaces, we perform two different electrochemical treatments. The first one, at low current density, has been proved to lead to the deposition of an "$InPO_4$-like" oxide few nanometers thick, according to the experimental conditions described in Ref. 35. The second one, at higher current density, leads to the deposition of a much thicker oxide and is detailed in Ref. 35 as well.

Prior to any electrochemical treatment, the InP surfaces are mechanochemically polished for 2 min with a Br_2 (2%)/methanol solution and rinsed with pure methanol. Then, to remove any residual oxide, the samples are dipped for few minutes in 2 M HCl, just before the electrochemical treatment.

The electrochemical treatment of the InP surfaces is performed in a borate buffered Tritisol (Merck) solution at pH 9, using a classical three-electrode configuration with a mercury sulfate electrode ($E_{MSE} = +0.65$ V/SHE) as reference electrode and a Pt counter electrode.

Oxidation treatments are performed by applying a constant anodic current density J_a at the electrode interface (galvanostatic mode). In particular, two values of current density are used, $J_a = 0.2$ mA.cm^{-2} and $J_a = 12$ mA.cm^{-2}, with a treatment duration of 900 and 120 s, respectively.

Electrochemical measurements of the surfaces treated with low current density, $J_a = 0.2$ mA.cm^{-2}, are performed as a probe of the oxide deposition as well as of the electrical properties of the oxide itself. In particular, capacitance versus potential measurements are carried out in the dark before and after the treatment. They are used as an *in situ* probe of oxidation, and of the thickness, the chemical properties, and the electrical quality of the deposited oxide layer. After the electrochemical treatment, the capacitance versus potential curves are nearly flat, as is shown in Fig. 3. This behavior indicates a quasiconstant capacity response, which has clearly been related to the presence of an electrolyte, oxide, and semiconductor junction.[35] This result indicates that, after the electrochemical treatment, the InP surfaces are fully covered by a thin oxide layer, with a thickness of the order of $d = 5$ nm. According to the procedure described in Ref. 35, we can identify the thin oxide layer deposited on the InP surface with a nonstoichiometric oxide layer made of an indium phosphate-like film at the interface covered by an indium-rich layer.

Electrochemical treatments implying a high current density, $J_a = 12$ mA.cm^{-2}, for a duration of 120 s, lead to the deposition of an oxide layer a few tens of nanometers thick.[35] Such oxides are characterized by a strong indium enrichment compared to the thin ones. Although the exact stoichiometric composition of these oxides is unknown, previous results suggest that an external indium-rich layer is present.[35] Such oxides may be affected by heterogeneity at the surface.
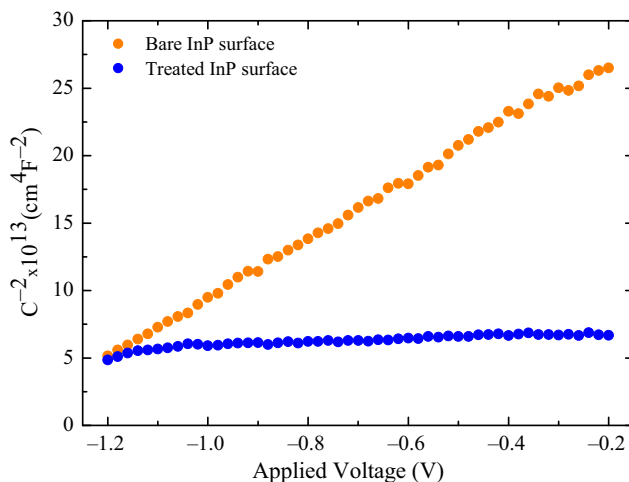

Fig. 3 Capacitance versus potential curve of a InP surface electrochemically treated with a current $J_a = 0.2$ mA.cm^{-2} during 900 s before (orange curve) and after the anodic treatment (blue curve).

We also study the commercial InP surfaces provided by the company InPact and covered by an $InP_{0.6}O_{2.5}$ oxide layer, whose thickness is of the order of $d = 1$ nm, providing a thinner oxide spacer between the deposited NCs and the InP surface. The InP substrates are n-doped, with a dopant concentration of $10^{18}/cm^3$, and are used as received.

3.2 CdSe/CdS Nanocrystals

The NCs, synthesized according to an organometallic procedure using a modification of the method described in Ref. 36, are core/shell CdSe/CdS NCs ($\lambda = 620$ nm peak emission at room temperature, full width at half maximum of 30 nm) with a core diameter of about 3 nm and a CdS shell of nominal thickness of the order of 4 nm, resulting in a final size of about 10 nm. On the representative transmission electron microscopy (TEM) image shown in Fig. 4(a), one can observe a slight dispersion in the size of the NCs. The histogram of Fig. 4(b), obtained measuring the diameters of the NCs in several TEM images, shows that the diameters of the NCs range between 8 and 14 nm. The peripheral layer of organic ligands is constituted of hexadecylamines and oleates, with a length of about 2 nm. The final diameters of the NCs fluctuate, therefore, between 12 and 18 nm.

3.3 Experimental Setup

The experimental setup has been described elsewhere.[37] Briefly, it consists of a confocal microscope with an air objective of numerical aperture 0.95. Pulsed excitation comes from a pulsed laser diode with $\lambda_{exc} = 485$ nm (Picoquant, LDH P-C-485). The pulse duration (70 ps) is much shorter than the radiative lifetime of the NCs (few tens of ns, see below), which allows to observe single photon emission coming from the recombination of the exciton state. The repetition period of the excitation ranges between 100 and 400 ns. It is tuned to get the maximum intensity while being an order of magnitude longer than the PL lifetime in order to allow the excited NC to relax to the ground state between two successive excitations. The backreflected signal of the laser is removed from the PL signal through a bandpass filter (630/60 nm), and the parasite signal, which might arise from the InP surface, is suppressed with an 800-nm shortpass filter. The photons are detected by a high sensitivity Hanbury Brown and Twiss setup, which consists of two avalanche photodiodes (PerkinElmer, time resolution of 300 ps). Each of the signals of the two photodiodes is sent to a data acquisition card (PicoHarp 300). All measurements are performed at room temperature.

3.4 Photoluminescence of Single CdSe/CdS NCs

We investigate ET between single NCs and InP surfaces by studying how the PL decay lifetimes of the NCs are affected by the proximity of the passivated InP surface. We first characterize the
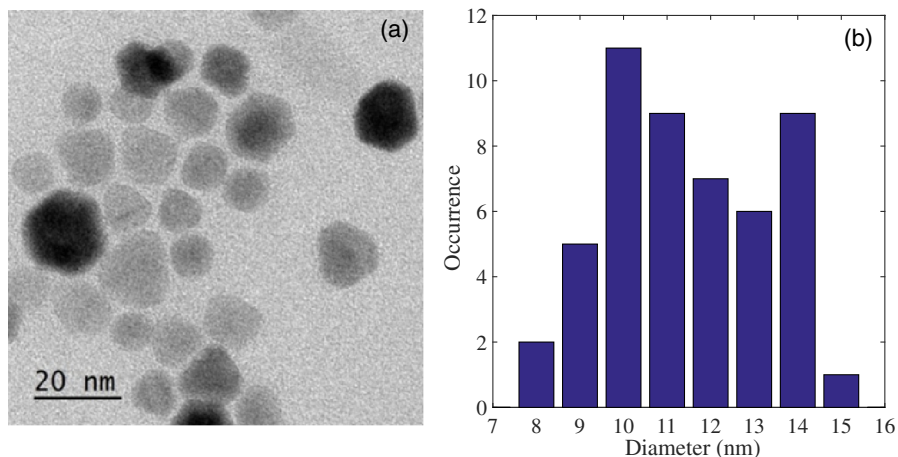

Fig. 4 (a) TEM image of the CdSe/CdS NCs and (b) histogram of the diameters of the NCs.

PL decay lifetimes of the NCs on a glass surface. For this purpose, a nanomolar solution is spin-coated on a glass coverslip and the PL decay lifetimes of the NCs are measured. The low concentration of NCs in the deposited solution strongly reduces the occurrence of aggregated NCs. A region of the surface that is a few μm^2 large is excited with an ultraviolet lamp, and a camera based on a charge coupled device provides a wide field image, which serves as the starting point to select the NCs to investigate. Under pulsed laser excitation, we operate in a regime of constant counts. This ensures that a single emitter is excited rather than an aggregate of several emitters. Indeed, in the last case, we would expect strong fluctuations of the photons counted under the same excitation conditions. For a second time, a nanomolar solution is spin-coated on the passivated InP surface and the PL decay lifetimes of single NCs are measured with the same procedure. The PL decays of tens of single NCs on glass and on each passivated surface are measured. In view of the interpretation of our experimental results, we point out that the spin-coat procedure that we use allows a control on the NC—interface distance within around 5 nm.[38]

We observe that the PL decays of single CdSe/CdS NCs on glass are not monoexponential. Most decays are well fitted with a biexponential curve, giving two characteristic lifetimes, which have been unambiguously associated with the neutral exciton (longest decay lifetime) and the ionized exciton (trion, shortest decay lifetime) in previous studies on NCs with core and shell characteristics comparable with those of the ones investigated here.[37,39] When dealing with a multiexponential decay, it is useful to determine the average lifetime, which is given by the equation $\tau_m = \dfrac{\sum_i A_i \tau_i^2}{\sum_i A_i \tau_i}$, where τ_i is the decay time and A_i, at $t = 0$, the amplitude of the i'th component of the multiexponential decay.[1,2,40] We find that the relative weights of the neutral

Fig. 5 (a) PL decays of single NCs on glass (gray line) and on the passivated InP surfaces with oxide thickness $d = 5$ nm (green line) and $d =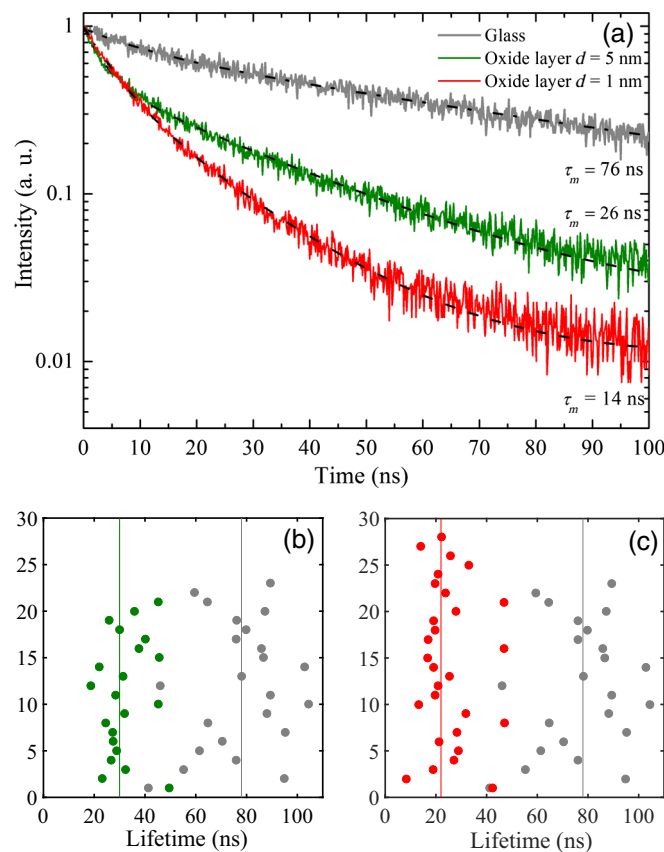 1$ nm (red line). Distribution of the mean lifetimes extracted from the PL decays of single NCs on glass (gray circles) and on the passivated InP surfaces with oxide thickness (b) $d = 5$ nm and (c) $d = 1$ nm. The vertical lines represent the median values of the distributions of the mean lifetimes.

state and the ionized state in the measured decays vary from NC to NC within the ranges 0.6 to 0.9 and 0 to 0.3, respectively. This is an indication of the heterogeneity in the core/shell structure, which can be attributed to size fluctuations in the cores and/or to the properties of the passivating shell, as has been observed in CdSe/CdS NCs with similar characteristics.[41] The mean value of the distribution is $\tau_{mean}(glass) = 77 \pm 17$ ns.

The PL decay lifetimes of the NCs on the passivated InP surfaces are well fitted with a biexponential curve as well and the amplitudes of the components of the biexponential decays are also widely spread. Representative PL decays of single NCs on glass (gray line) and on the InP surfaces passivated with oxides of thickness $d = 5$ nm (green line) and $d = 1$ nm (red line) are shown in Fig. 5(a) together with the mean lifetimes extracted according to the equation introduced above. The mean lifetimes extracted from the PL decays of the NCs on the passivated InP surfaces are compared with those on glass in Figs. 5(b) and 5(c). The distributions of the mean lifetimes of the single NCs both on glass and on the passivated InP surfaces are quite wide [see Figs. 5(b) and 5(c) where the vertical lines represent the median values as a guide for the eye]. We would like to emphasize again that this is due to the dispersion in the structural properties of the NCs (core size and shell thickness) that manifest themselves when dealing with NCs at the single level. Overall, our results show a clear shortening of the PL decay lifetimes of single NCs deposited on passivated InP surfaces compared to glass. This becomes clear by comparing the mean values of the distributions on the passivated InP surfaces, which are, respectively, $\tau_{mean}(d = 5 \text{ nm}) = 32 \pm 9$ ns and $\tau_{mean}(d = 1 \text{ nm}) = 25 \pm 10$ ns, with the mean value of the distribution on glass. The shortening of the PL decay lifetimes of the single NCs will be discussed in detail in Sec. 4.

4 Discussion

The shortening of the PL decay lifetimes of single NCs on InP compared to glass, shown in Figs. 5(b) and 5(c), strongly suggests the opening of recombination pathways for the photogenerated exciton. Size dispersion, together with the study of the PL decays of single NCs, results in widely distributed lifetimes. A further source of dispersion in the lifetime distributions is due to the fact that we do not measure the lifetime of the same NC on glass and on InP, but the comparisons between the lifetimes are made on different NCs.

As we have discussed in Sec. 2, the spontaneous emission rate of a 2-D dipole in close vicinity of a dielectric interface depends not only on the distance from the interface itself, but also on the orientation of the emitter with respect to the plane of the interface.

The random orientation of the NCs on the InP surfaces, together with the study of single NCs, enables us to explore a much wider range of coupling regimes between the NCs and the InP surface compared to the ensemble measurements, where such effects are averaged over the distributions of size and orientation of the NCs. From the mean lifetimes of the PL decays of single NCs on glass and on InP shown in Figs. 5(b) and 5(c), we determine all the possible values of $\alpha = \frac{k_{InP}}{k_{glass}} = \frac{\tau_{glass}}{\tau_{InP}}$, where τ_{glass} and τ_{InP} span over all the measured lifetimes, which we compare with the theoretical values of α as determined in Sec. 2.

For the InP surface passivated with a $d = 1$-nm-thick oxide layer, most of the α lie within the range $3 < \alpha < 4.75$, and the mean value averaged over all the experimental values is $\alpha_{mean} = 3.6$. The value $\alpha_{min} = 3$ (open square in Fig. 6) is consistent with the emission of a dipole with both the orthogonal components oriented parallel to the interface and the value $\alpha_{max} = 4.75$ (full square in Fig. 6) is consistent with a dipole with a component parallel to the interface and a component perpendicular to the interface, both located at the same distance from the interface, $d = 6$ nm. Taking into account the distance between the NC and the InP surface introduced by the spin-coating deposition, which can be estimated to around 5 nm, the value of 6 nm, which we find for the total distance between the NC and the InP surface, is consistent with the thickness of the deposited oxide layer $d = 1$ nm.

We calculate all the possible values of α from the lifetimes of single NCs on the InP surface with a $d = 5$-nm-thick oxide layer. In this case, most of the α lie within the range $2.5 < \alpha < 4$ and the mean value is $\alpha_{mean} = 2.6$. The extreme values of this interval, $\alpha_{min} = 2.5$ (open circle in Fig. 6) and $\alpha_{max} = 4$ (full circle in Fig. 6), are consistent, respectively, with the emission of a
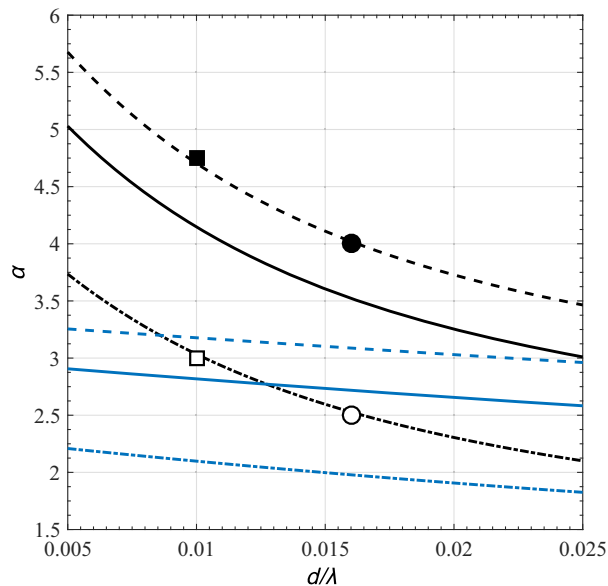
Fig. 6 Zoom of the curves represented in Fig. 2 (black lines) showing the calculation of α for $z = 12$ nm and $\lambda = 620$ nm as a function of the thickness of the passivating oxide layer normalized to the emission wavelength of the NCs, d/λ, for an ensemble of dipoles of random orientation $\langle \alpha \rangle = \frac{2}{3}\alpha_{\parallel} + \frac{1}{3}\alpha_{\perp}$ (plain line), for a dipole with both the components lying in the plane of the interface $\alpha = \alpha_{\parallel}$ (dashed dotted line) and for a dipole with a component perpendicular to the plane of the inter-face and a component lying in the plane of the interface, $\alpha = \frac{1}{2}(\alpha_{\parallel} + \alpha_{\perp})$ (dashed line). The symbols represent the extreme values of the experimental ranges of α for $d = 1$ nm (squares) and for $d = 5$ nm (circles). The curves corresponding to a pure dielectric substrate of permittivity $\varepsilon(\text{InP}) = 12.493$ are also shown in light blue.

dipole whose orthogonal components are both parallel to the interface and a dipole with a component parallel to the interface and a component perpendicular to the interface, both located at a distance of $d = 10$ nm from the interface itself. Here again the result is consistent with a $d = 5$-nm-thick oxide layer, if we take into account the distance between the NCs and the InP surface due to the spin-coating deposition.

Thus, for NCs located at the same distance from the oxide/InP interface, the coupling and the ET to the InP surface is strongly dependent on the orientation of the NC with respect to the interface itself.

We need to remind that the decay rate of the excited NC is affected not only by the ET to the semiconductor surface, but also by the modification of the spontaneous decay rate induced by the surface itself, which occurs even for a pure dielectric substrate.[42,43]

To exclude that the shortening of the PL decay lifetimes observed here is solely due to the modification of the emission rate in the far field caused by the substrate, we evaluate the expressions of $\alpha = \alpha_{\parallel}$ and $\alpha = \frac{1}{2}(\alpha_{\parallel} + \alpha_{\perp})$ for a pure dielectric substrate of permittivity $\varepsilon(\text{InP}) = 12.493$, which are shown in Fig. 6 together with the expression for the case of an ensemble of randomly oriented dipoles $\langle \alpha \rangle = \frac{2}{3}\alpha_{\parallel} + \frac{1}{3}\alpha_{\perp}$ (light blue curves). The comparison between these curves and the corresponding ones for the passivated InP surfaces shows clearly that NRET to the substrate has to be taken into account in order to explain the shortening of the PL decay lifetimes observed.

Finally, we measure the PL decay lifetimes of single NCs spin-coated on an InP surface coated with a thick oxide layer (few tens of nanometers), grown according to the procedure described in Sec. 3.1.

The histogram of Fig. 7 reveals that most of the values of α lie within the interval $\alpha_{\min} = 1.5$ and $\alpha_{\max} = 2.5$. By looking at the curves in Fig. 2, it is clear that the distance between the NCs and the surface is larger than 40 nm. This result is in qualitative agreement with the results discussed above and is consistent with a thick and heterogeneous oxide layer passivating the InP surface (see Sec. 3.1).
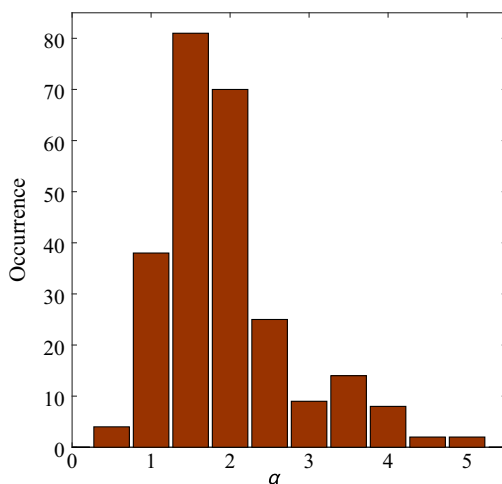
Fig. 7 Distribution of the α calculated from all the measured lifetimes of single NCs on glass and on an InP surface electrochemically passivated with a thick oxide layer, $d > 10$ nm.

5 Conclusion

In this paper, we have shown that the PL decay lifetimes of single NCs are modified by the deposition on InP surfaces passivated with an oxide layer few nanometers thick. The shortening of the PL decay lifetimes demonstrates the opening of a recombination channel for the photo-generated exciton, which we have attributed to the transfer of the exciton energy to electron–hole pairs in the semiconductor layer. The study of surfaces passivated with oxides of different thicknesses has enabled us to show how the distance between the NC and the InP surface affects the PL decays.

Measuring the PL decays of single NCs, together with size distribution and random orientation of the NCs with respect to the passivated surfaces, results in a wide distribution of the shortened lifetimes. Different regimes of coupling of the NCs with the surfaces have been revealed, providing insight on the modification of the radiative decay of an emitter in close vicinity of a dielectric interface. This phenomenon, interesting for itself, can be advantageous for the conception of hybrid photovoltaic cells based on ET and for external sensitization of inorganic semiconductors.

Acknowledgments

References

1. J. R. Lakowicz, *Principles of Fluorescence Spectroscopy*, 3rd ed., Springer, New York (2006).
2. B. Valeur, *Molecular Fluorescence: Principles and Applications*, Wiley-VCH Verlag GmbH, Weinheim, Germany (2001).
3. T. Förster, "Zwischenmolekulare energiewanderung und fluoreszenz," *Ann. Phys.* **437**(1–2), 55–75 (1948).
4. D. L. Dexter, "Two ideas on energy transfer phenomena: ion-pair effects involving the OH stretching mode, and sensitization of photovoltaic cells," *J. Lumin.* **18**, 779–784 (1979).
5. M. Stavola, D. L. Dexter, and R. S. Knox, "Electron–hole pair excitation in semiconductors via energy transfer from an external sensitizer," *Phys. Rev. B* **31**(4), 2277–2289 (1985).
6. R. R. Chance, A. Prock, and R. Silbey, "Comments on the classical theory of energy transfer," *J. Chem. Phys.* **62**(6), 2245–2253 (1975).
7. H. M. Nguyen et al., "Spectroscopic evidence for nonradiative energy transfer between colloidal CdSe/ZnS nanocrystals and functionalized silicon substrates," *Appl. Phys. Lett.* **98**(16), 161904 (2011).

8. H. M. Nguyen et al., "Efficient radiative and nonradiative energy transfer from proximal CdSe/ZnS nanocrystals into silicon nanomembranes," *ACS Nano* **6**(6), 5574–5582 (2012).

9. M. T. Nimmo et al., "Visible to near-infrared sensitization of silicon substrates via energy transfer from proximal nanocrystals: further insights for hybrid photovoltaics," *ACS Nano* **7**(4), 3236–3245 (2013).

10. M. Achermann et al., "Energy-transfer pumping of semiconductor nanocrystals using an epitaxial quantum well," *Nature* **429**(6992), 642–646 (2004).

11. Š. Kos et al., "Different regimes of Förster-type energy transfer between an epitaxial quantum well and a proximal monolayer of semiconductor nanocrystals," *Phys. Rev. B* **71**(20), 205309 (2005).

12. S.-S. Sun and N. S. Sariciftci, *Organic Photovoltaics: Mechanisms, Materials, and Devices*, CRC Press, Boca Raton, Florida (2005).

13. C. A. Leatherdale et al., "On the absorption cross section of CdSe nanocrystal quantum dots," *J. Phys. Chem. B* **106**(31), 7619–7622 (2002).

14. C. B. Murray, C. R. Kagan, and M. G. Bawendi, "Synthesis and characterization of monodisperse nanocrystals and close-packed nanocrystal assemblies," *Annu. Rev. Mater. Sci.* **30**(1), 545–610 (2000).

15. M. Bruchez et al., "Semiconductor nanocrystals as fluorescent biological labels," *Science* **281**(5385), 2013–2016 (1998).

16. V. I. Klimov et al., "Optical gain and stimulated emission in nanocrystal quantum dots," *Science* **290**(5490), 314–317 (2000).

17. C. W. Wilmsen, *Physics and Chemistry of III-V Compound Semiconductor Interfaces*, Plenum, New York (1985).

18. M. Levinstein, S. Rumyantsev, and M. Shur, Eds., "Handbook series on semiconductor parameters," Vol. **1**–**2**, World Scientific, London (1999).

19. W. Lukosz and R. E. Kunz, "Light emission by magnetic and electric dipoles close to a plane dielectric interface. II. Radiation patterns of perpendicular oriented dipoles," *J. Opt. Soc. Am.* **67**(12), 1615–1619 (1977).

20. W. Lukosz, "Light emission by magnetic and electric dipoles close to a plane dielectric interface. III. Radiation patterns of dipoles with arbitrary orientation," *J. Opt. Soc. Am.* **69**(11), 1495–1503 (1979).

21. K. H. Drexhage, H. Kuhn, and F. P. Schäfer, "Variation of the fluorescence decay time of a molecule in front of a mirror," *Ber. Bunsengesellschaft Phys. Chem.* **72**(2), 329 (1968).

22. K. Tews, O. Inacker, and H. Kuhn, "Variation of the luminescence lifetime of a molecule near an interface between differently polarizable dielectrics," *Nature* **228**(5268), 276–278 (1970).

23. W. Lukosz and R. E. Kunz, "Light emission by magnetic and electric dipoles close to a plane interface. I. Total radiated power," *J. Opt. Soc. Am.* **67**(12), 1607–1615 (1977).

24. A. L. Efros et al., "Band-edge exciton in quantum dots of semiconductors with a degenerate valence band: dark and bright exciton states," *Phys. Rev. B* **54**(7), 4843–4856 (1996).

25. J. D. Jackson, *Classical Electrodynamics*, Wiley, New York (1962).

26. L. Novotny and B. Hecht, *Principles of Nano-Optics*, Cambridge University Press, Cambridge, United Kingdom (2012).

27. D. E. Aspnes and A. A. Studna, "Dielectric functions and optical parameters of Si, Ge, GaP, GaAs, GaSb, InP, InAs, and InSb from 1.5 to 6.0 eV," *Phys. Rev. B* **27**(2), 985–1009 (1983).

28. M. J. Weber, *Handbook of Optical Materials*, CRC Press, Boca Raton, Florida (2003).

29. N. Simon et al., "Thin anodic oxides on n-InP studied by photocurrent transients and surface analysis," *Thin Solid Films* **400**(1), 134–138 (2001).

30. M. P. Besland, Y. Robach, and J. Joseph, "*In situ* studies of the anodic oxidation of indium phosphide," *J. Electrochem. Soc.* **140**(1), 104–108 (1993).

31. P. Louis et al., "Correlations between the electrical characteristics of metal-oxide-InP tunnel diodes and the nature of thin interfacial oxides," *J. Electrochem. Soc.* **142**(4), 1343–1348 (1995).

32. G. Hollinger et al., "On the nature of oxides on InP surfaces," *J. Vac. Sci. Technol. A* **3**(6), 2082–2088 (1985).

33. J. Joseph, A. Mahdjoub, and Y. Robach, "Propriétés électriques des structures MIS sur InP passivé par un oxyde," *Rev. Phys. Appl. Paris* **24**(2), 189–194 (1989).

34. N. Simon, N. C. Quach, and A. Etcheberry, "Growth of anodic oxides on n-InP studied by electrochemistry and surface analysis. Correlation between oxidation methods and passivating properties," in *Proc. Electrochemical Society*, Vol. 2003, No. 4, pp. 73–82 (2003).

35. N. Simon et al., "Growth of anodic oxides on n-InP studied by electrochemical methods and surface analyses," *J. Electrochem. Soc.* **154**(5), H340 (2007).

36. B. Mahler et al., "Towards non-blinking colloidal quantum dots," *Nat. Mater.* **7**(8), 659–664 (2008).

37. P. Spinicelli et al., "Bright and grey states in CdSe-CdS nanocrystals exhibiting strongly reduced blinking," *Phys. Rev. Lett.* **102**(13), 136801 (2009).

38. W. Peng et al., "Silicon surface modification and characterization for emergent photovoltaic applications based on energy transfer," *Chem. Rev.* **115**(23), 12764–12796 (2015).

39. D. Canneson et al., "Strong Purcell effect observed in single thick-shell CdSe/CdS nanocrystals coupled to localized surface plasmons," *Phys. Rev. B* **84**(24), 245423 (2011).

40. E. Fišerová and M. Kubala, "Mean fluorescence lifetime and its error," *J. Lumin.* **132**(8), 2059–2064 (2012).

41. F. Federspiel et al., "Distance dependence of the energy transfer rate from a single semiconductor nanostructure to graphene," *Nano Lett.* **15**(2), 1252–1258 (2015).

42. A. N. Poddubny and A. V. Rodina, "Nonradiative and radiative Förster energy transfer between quantum dots," *J. Exp. Theor. Phys.* **122**(3), 531–538 (2016).

43. V. M. Agranovich, Y. N. Gartstein, and M. Litinskaya, "Hybrid resonant organic–inorganic nanostructures for optoelectronic applications," *Chem. Rev.* **111**(9), 5179–5214 (2011).

Biographies for the authors are not available.